RSC Advances

ROYAL SOCIETY OF CHEMISTRY

www.rsc.org/advances

Journal Name

RSCPublishing

ARTICLE

Hydriding characteristics of $NaMgH_2F$ with Preliminary Technical and Cost Evaluation of Magnesium-Based Metal Hydride Materials for Concentrating Solar Power Thermal Storage

Cite this: DOI: 10.1039/x0xx00000x

Received 00th January 2012,
Accepted 00th January 2012

DOI: 10.1039/x0xx00000x

www.rsc.org/

D.A. Sheppard,[a] C. Corgnale,[b] B. Hardy,[b] T. Motyka,[b] R. Zidan,[b] M. Paskevicius and C.E. Buckley[a],

A simplified techno-economic model has been used as a screening tool to explore the factors that have the largest impact on the costs of using metal hydrides for concentrating solar thermal storage. The installed costs of a number of paired metal hydride concentrating solar thermal storage systems were assessed. These comprised of magnesium-based (MgH_2, Mg_2FeH_6, $NaMgH_3$, $NaMgH_2F$) high-temperature metal hydrides (HTMH) for solar thermal storage and $Ti_{1.2}Mn_{1.8}H_{3.0}$ as the low-temperature metal hydride (LTMH) for hydrogen storage. A factored method approach was used for a 200 MW_{el} power plant operating at a plant capacity factor (PCF) of 50% with 7 hours of thermal storage capacity at full-load. In addition, the hydrogen desorption properties of $NaMgH_2F$ have been measured for the first time. It has a practical hydrogen capacity of 2.5 wt.% (2.95 wt.% theoretical) and desorbs hydrogen in a single-step process above 478 ^oC and in a two-step process below 478 ^oC. In both cases the final decomposition products are $NaMgF_3$, Na and Mg. Only the single-step desorption is suitable for concentrating solar thermal storage applications and has an enthalpy of 96.8 kJ/mol.H_2 at the midpoint of the hydrogen desorption plateau. The techno-economic model showed that the cost of the LTMH, $Ti_{1.2}Mn_{1.8}H_{3.0}$, is the most significant component of the system and that its cost can be reduced by increasing the operating temperature and enthalpy of hydrogen absorption in the HTMH that, in turn, reduces the quantity of hydrogen required in the system for an equivalent electrical output. The result is that, despite the fact that the theoretical thermal storage capacity of $NaMgH_2F$ (1416 kJ/kg) is substantially lower than the theoretical values for MgH_2 (2814 kJ/kg), Mg_2FeH_6 (2090 kJ/kg) and $NaMgH_3$ (1721 kJ/kg), its higher enthalpy and operating temperature leads to the lowest installed cost of the systems considered. A further decrease in cost could be achieved by utilizing metal hydrides with yet higher enthalpies and operating temperatures or by finding a lower cost option for the LTMH.

1. Introduction

Solar energy is the most abundant clean and renewable alternative to fossil fuels.[1] However, achieving its widespread use will only be possible if the costs of solar energy storage and electricity production are significantly reduced. While the cost of solar photovoltaics (PV) is decreasing rapidly,[2] storing the electricity produced by PVs in electrochemical batteries is a high-cost option. An alternative option is to use concentrating solar thermal (CST) technologies and to store the energy as heat that can be accessed on demand to generate electricity. The cost of solar thermal heat storage is a critical factor in its future

deployment and there are two strategies for reducing its cost: 1) utilizing higher energy density storage materials to reduce the volume and mass of the material and system required and; 2) utilizing higher energy storage temperatures to increase overall solar to electricity conversion efficiencies.[3]

The three main methods of thermal energy storage use; (1) the sensible heat (or heat capacity) of materials; (2) the phase change heat (or latent heat of fusion) of materials and; (3) reversible thermochemical reactions. Sensible heat materials, such as the eutectic molten salt $NaNO_3/KNO_3$, can store ~150 kJ/kg of heat per 100 ^oC,[4] whilst phase change materials, such as $NaNO_3$, can store ~199 kJ/kg of heat during melting.[5] Thermochemical candidates, such as those involving the partial oxidation of metals, can store 200 - 850 kJ/kg of heat.[4] In the case of phase change and thermochemical candidates, their total heat storage capacity can also be supplemented by a sensible heat contribution. An alternative class of thermochemical candidates is represented by metal hydrides.[3] A wide range of compounds in this class can reversibly react with hydrogen gas over a wide range of temperatures and have substantially higher theoretical heat storage capacities than other thermochemical candidates. These compounds range from Mg_2NiH_4 with an operating temperature of 260 ^oC - 400 ^oC and a theoretical heat storage capacity of 1117 kJ/kg [6] to LiH with an operating temperature above 850 ^oC and a theoretical heat storage capacity of 8397 kJ/kg. Including the sensible heat of the metal hydrides adds another 4-7% of heat storage capacity for every 50 ^oC of operating temperature range. The low cost of magnesium means that a range of Mg-based metal hydrides, such as Mg_2NiH_4, MgH_2, Mg_2FeH6, Mg_2CoH_5 [6] and $NaMgH_3$,[7] have been considered as heat storage candidates. A further advantage of metal hydrides as a thermal storage medium for CSP is that they can potentially operate at temperatures above 600 ^oC where molten salts would decompose.[8]

The use of metal hydrides for concentrating solar thermal energy storage requires a system of paired metal hydrides:[9] the high-temperature metal hydride (HTMH) as the heat storage medium and a low-temperature metal hydride (LTMH) for hydrogen (H_2) storage. During periods of sunlight, incoming solar radiation is focused by mirrors to generate heat. Part of this heat is transferred to a heat engine to generate electricity and part of the heat is directed to the HTMH to release H_2 in an endothermic reaction, with the released H_2 temporarily stored in the LTMH or in a compressed gas tank. During night time or periods of cloud cover, the reactor temperature of the HTMH hydride begins to fall, causing the system pressure to drop and H_2 is consequently released from the LTMH and absorbed by the HTMH in a self-regulating cycle. This absorption by the HTMH hydride is an exothermic reaction that can be used to drive the heat engine and generate electricity.[3] The reader is referred to the literature for further details.[3,9]

In basic terms, the total cost for a paired metal hydride solar thermal energy storage system can be calculated based on: 1) the raw materials cost of both the HTMH and LTMH; 2) the heat transfer system and pressure vessel installed cost for both the HTMH and LTMH. In particular the HTMH material cost is determined by: the raw material price for the metal hydride and its mass, which is a function of its hydrogen capacity, the heat released during hydrogen absorption (enthalpy of absorption, ΔH_{abs}) and the operating temperature and efficiency of the power plant. The cost of the LTMH is also determined by its raw material price, its hydrogen capacity and the quantity of hydrogen to be stored. The quantity of hydrogen to be stored, and hence the quantity and cost of the LTMH, can be reduced by using a HTMH with a higher enthalpy of hydrogen absorption/desorption and increasing the efficiency of the power plant by operating at higher temperature. In the ideal scenario the HTMH would be cheap, with maximized hydrogen capacity, enthalpy of absorption and operating temperature while the LTMH would be cheap with a large hydrogen capacity and a low enthalpy of hydrogen absorption. In practice, most LTMH candidate materials are intermetallic alloys with modest hydrogen capacity (<2.0 wt.% H_2) and high-cost components such as titanium, zirconium, vanadium, lanthanum etc.[3] They, therefore, have the potential to add substantial cost to a solar thermal storage system based on metal hydrides.

The benefit of employing HTMHs with higher enthalpies and operating temperatures, to reduce the amount of hydrogen that must be stored in the LTMH hydride, is illustrated by the equation for the Practical Carnot Efficiency (PCE) of electricity generation.[10] For most metal hydrides, the entropy of hydrogen absorption is relatively constant (ΔS ~ 134 J/mol.H_2.K) and so by defining the high temperature of the heat engine (T_h) to be the 1 bar H_2 desorption temperature of the HTMH (given by $T_h = \Delta H/\Delta S$) then the efficiency of the heat engine can be related to the enthalpy of hydrogen absorption/desorption, ΔH, by Equation 1:

$$\text{PCE} = 1 - (T_c/T_h)^{1/2}$$

$$= 1 - (\Delta S.T_c/\Delta H)^{1/2}$$

$$= 1 - (134.T_c/\Delta H)^{1/2} \qquad \text{Equation 1}$$

Where T_c is the heat sink temperature of the heat engine, in K, (assumed to be 303 K = 30 ^oC), T_h is the operating temperature of the heat engine assumed equal to the HTMH desorption temperature (at 1 bar H_2), in K, and ΔH is the enthalpy of desorption in J/mol.H_2. This equation is not definitive and should only be used as a guide because the entropy of some hydrides deviates substantially from 134 J/mol.H_2.K, such as Mg_2NiH_4 (122 J/mol.H_2.K)[11] and LiH (173 J/mol.H_2.K).[12] It should also be noted that Equation 1 is a continuous function for evaluating power plant efficiency but, in reality there are 'fixed' values of power plant efficiency that depend not only on the temperature but also on the type of plant and the state of the art.

The relationship between the enthalpy of hydrogen desorption for the HTMH hydride and the amount of hydrogen that must be stored in the LTMH hydride is represented in Figure 1. For example, changing the enthalpy of desorption of the HTMH

from 75 kJ/mol.H_2 to 90 kJ/mol.H_2 reduces the amount of H_2 that must be stored and the amount of LTMH required by ~50%.

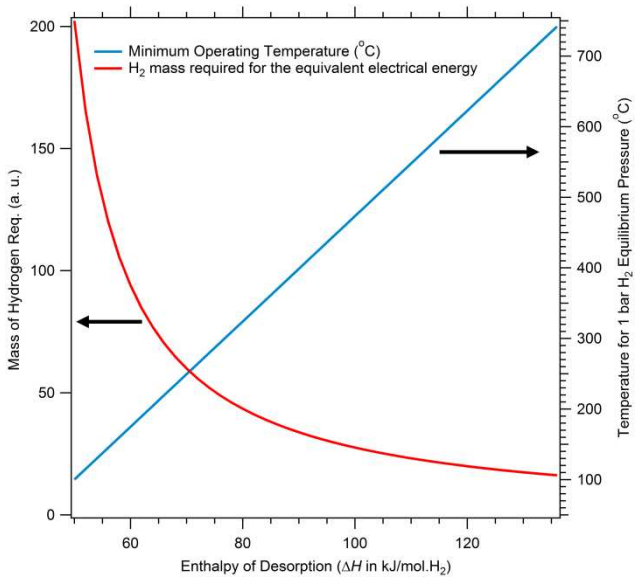

Fig 1 The amount of H_2 required to generate an equivalent amount of electricity as a function of the enthalpy of hydrogen desorption, ΔH, and the minimum operating temperature for the HTMH.

The perovskite metal hydride, $NaMgH_3$,[13-15] has recently been considered as a solar thermochemical heat storage medium.[7] $NaMgH_3$ releases hydrogen in a two-step process:

$NaMgH_3 \rightarrow NaH + Mg + H_2$ (g) Equation 2

$NaH \rightarrow Na(l) + H_2$ (g) Equation 3

Equation 2 releases 4.0 wt% of hydrogen with an enthalpy of 86.6 kJ/mol H_2 [7] (1721 kJ/kg) and Equation 3 releases a further 2.0 wt.% of hydrogen with an enthalpy of 117 kJ/mol H_2 (1160 kJ/kg) for a total hydrogen capacity of 6.0 wt.% and a theoretical thermal energy storage capacity of 2881 kJ/kg. This capacity exceeds the theoretical value of both MgH_2 (2814 kJ/kg) and Mg_2FeH_6 (2090 kJ/kg). The higher enthalpy of hydrogen desorption means that higher operating temperatures can be used with $NaMgH_3$ at lower hydrogen pressures. One drawback of $NaMgH_3$ is that full hydrogen desorption results in molten sodium metal segregation with poor kinetics during hydrogen reabsorption.[7,16] However if only the first hydrogen desorption step is employed (Equation 2) then the kinetics of hydrogen absorption are not impeded[7] but the total hydrogen capacity and thermal storage capacity are limited to a theoretical maximum of 4.0 wt.% and 1721 kJ/kg, respectively. Additionally, the thermodynamics of Equation 2 and Equation 3 suggest that they will have the same H_2 desorption pressure between ~580 °C and ~600 °C. The result will be that the reaction will combine into a single desorption event between 580°C and 600°C. In the case of $KMgH_3$, the transformation to a single desorption plateau was followed by limited reversibility. that may hinder its high temperature viability.[17] A similar transformation to a single desorption plateau in the $NaMgH_3$ system may hinder its practical application at high temperatures.

One approach to alter the properties of $NaMgH_3$ is to partially substitute fluorine for hydrogen to form $NaMgH_2F$. This substitution has been shown to stabilize the structure relative to pure $NaMgH_3$[14] and should increase the enthalpy of hydrogen absorption/desorption, increase the minimum operating temperature (T_h) of the HTMH and decrease the amount of hydrogen that needs to be stored in the LTMH. If the decomposition reaction is similar to Equation 2 then the formation of molten Na can be avoided and H_2 absorption kinetics improved (Equation 4):

$NaMgH_2F \rightarrow NaF + Mg + H_2$ (g) Equation 4

Here we first examine the hydrogen desorption/absorption properties of $NaMgH_2F$ and consider its suitability as a high-temperature concentrating solar thermal storage medium when paired with $Ti_{1.2}Mn_{1.8}H_{3.0}$ (originally reported as $TiMn_{1.5}H_{2.5}$)[18] as the LTMH. A model has been devised to perform preliminary estimates of the engineering costs for the solar thermal storage system based on paired metal hydrides for a 200 MW power plant operating at a plant capacity factor (PCF) of 50% and with 7 h of full-load thermal storage. Comparisons are made between $NaMgH_2F$ and other potential low-cost Mg-based metal hydride concentrating solar thermal storage materials (MgH_2, Mg_2FeH_6, $NaMgH_3$).

2. Experimental

Materials synthesis

All handling of chemicals and sealable milling canisters was undertaken in an argon-atmosphere glovebox in order to minimize oxygen (O_2 < 1 ppm) and water (H_2O < 1 ppm) contamination. $NaMgH_2F$ was synthesized by cryomilling NaH (98%, Sigma-Aldrich), MgH_2 (>96.5%, Sigma-Aldrich) and MgF_2 (99.9%, Sigma-Aldrich) at 77 K for 30 min in a Spex 6850 Freezer Mill. The choice of milling conditions and reagents was a matter of convenience based on sample size and chemical availability within our laboratory. Ball-milling NaF and MgH_2 at room-temperature would be equally effective. Following milling the sample was annealed under a H_2 pressure of 58 bar at 300 °C overnight. NaH and MgH_2 were added in a slight excess to account for their lower purity compared to MgF_2. X-ray Diffraction (XRD) was performed using a Bruker D8 Advance diffractometer (Cu Kα radiation) utilising XRD sample holders comprised of a poly(methylmethacrylate) (PMMA) airtight bubble to prevent oxygen/moisture contamination during data collection. The PMMA airtight bubble results in a broad hump in XRD patterns centered at ~20° 2θ. Diffraction patterns were quantitatively analyzed with the Rietveld method using the TOPAS software (Bruker-AXS). The hydrogen sorption properties were examined by measuring

Pressure-Composition-Isotherms (PCI) between 450 °C and 502 °C with a computer controlled Sieverts/volumetric apparatus previously described.[19] Briefly, the digital pressure transducer (Rosemount 3051S) had a precision and accuracy of 14 mbar, whilst room temperature measurements were recorded using a 4-wire platinum resistance temperature detector (RTD). The sample temperature was monitored using an N-type thermocouple that was calibrated by the manufacturer to be accurate to within 0.1 °C at 419 °C.

Above ~420 °C, the permeation of hydrogen directly through the walls of the stainless steel sample cell becomes an issue and the measured hydrogen content at each PCI data point has to be corrected for this loss. The hydrogen loss through the stainless steel sample cell can be calculated by the diffusional flux of hydrogen[20] (Equation 5), the dimensions of each of the stainless steel components that comprise the sample cell within the furnace, the pressure of the system and the duration for which the system is at a given pressure.

At the temperatures and hydrogen pressures used in this study there is negligible difference between the hydrogen fugacity and pressure. Consequently the hydrogen pressure can be substituted directly for the fugacity in calculating the steady state diffusional flux of hydrogen, Equation 5.[20]

$$J_{\infty} = \frac{\Phi}{t} P^{1/2}$$

Equation 5

Where J_{∞} = the steady state diffusional flux of hydrogen (in units of $mol.m^{-2}.s^{-1}$)

Φ = the permeability of hydrogen at a given temperature (in units of $mol.m^{-1}.s^{-1}.MPa^{-1/2}$)

t = the thickness of stainless steel (in units of m)

P = the pressure of hydrogen at a given temperature (in units of MPa)

The leak rate of hydrogen predicted by this method was verified by performing a pressure test over 15 h at a temperature of 450 °C and an initial hydrogen pressure of 14.01 bar. The pressure drop over this time period, as predicted with Equation 5, was 0.42 bar whilst the measured pressure drop was 0.415 bar. Based on the calculated leak rates, the duration of each data point in the PCI was limited to 2 h as a compromise between the kinetics of the sample and the hydrogen lost to diffusion through the stainless steel.

Method for Preliminary Techno-Economic Analysis of Metal hydride-based Solar Thermal Storage Systems

The adoption of $NaMgH_2F$ as the high temperature metal hydride material paired to a feasible low temperature metal hydride material was investigated, performing a preliminary conceptual design and economic evaluation and comparing the results with those obtained for other Mg-family materials. The new $NaMgH_2F$ material is still at a preliminary material development stage and will need further analyses and experimental activities (e.g. long term cycling) to evaluate its long term behavior as a potential thermal energy storage candidate. However further detailed analyses, both from experimental and modeling points of view, require strong efforts. Thus before carrying out detailed studies, preliminary screening analyses need to be carried out to evaluate the potential of new materials comparing the results with those obtained for other potential Mg-family based high temperature candidates. In particular, the present work uses the system installed cost as the primary function to evaluate and compare different metal hydride based storage systems.

To evaluate system installed costs a screening tool was developed at SRNL, which includes simplified system techno-economic models. An in-depth description of the tool is an object of another paper and goes beyond the scope of the present paper. However the main properties of the techno-economic models, as well as the analysis assumptions, will be highlighted in the present work.

The preliminary conceptual design and economic evaluation of the coupled metal hydride solar thermal storage systems have been carried out under the following assumptions:

- A 200 MW_{el} turbine is assumed to operate with a PCF factor of 50%, based on typical values of current solar plants,[21] corresponding to an average annual electric power output of 100 MW_{el};
- The storage time is equal to 7 hours at full load: similar to that for the Andasol Solar Power Station in Spain;
- The efficiency of the turbine has been assessed based on the practical Carnot efficiency equation;[10]
- The hydrogen capacity of each of the HTMH was based on practical values as discussed in the following sections and accounted for the addition of 5 wt.% Expanded Natural Graphite (ENG) used to improve the thermal conductivity of the metal hydride powders;
- The enthalpy of H_2 absorption/desorption for $Ti_{1.2}Mn_{1.8}H_{3.0}$ (LTMH) was assumed to be 28 $kJ/mol.H_2$ and its practical hydrogen capacity to be 1.7 wt.%;[18] It is also envisioned that the H_2 desorption from the LTMH will be driven by waste heat available from condensing steam from the steam power plant.
- The operating temperature range for Mg_2FeH_6, $NaMgH_3$ and $NaMgH_2F$ was chosen so that each of the systems had comparable hydrogen operating pressures that were compatible with $Ti_{1.2}Mn_{1.8}H_{3.0}$ operating at 25 °C. For $Ti_{1.2}Mn_{1.8}H_{3.0}$ the H_2 absorption pressure at 25 °C was assumed to be ~20 bar and the hydrogen desorption pressure at 25 °C was assumed to be ~8 bar;[18,22]
- The maximum operating temperature for MgH_2 is limited to 400 °C to avoid sintering effects and the resulting loss of capacity;[23] The enthalpy for $NaMgH_2F$ was taken to be the value at the midpoint of the desorption plateau;

The installed cost of the system has been assessed adopting a factored method approach.[24] The cost of the storage system accounts for (1) the cost of the metal hydride material and, based on previous experiences for small scale stationary applications,[25] an additional 20% that includes the cost due to handling, processing and placement of the material in the system (Table 1) and (2) the cost of the heat transfer system, which includes the cost of the heat exchanger, tube bundle and pressure vessel.

Table 1. Raw material costs used for techno-economic calculations.

Material	Raw Material Cost (US$/kg)	Processed Material Cost (US$/kg)
MgH_2[a]	3.00	3.60
Fe[b]	0.70	0.84
NaH[c]	4.00	4.80
NaF[d]	1.00	1.20
Mn[e]	2.93	3.52
Ti Sponge[f]	11.60	13.92
ENG[g]	1.60	1.92
Mg_2FeH_6	1.77	2.12
$NaMgH_3$	3.50	4.20
$NaMgH_2F$	1.73	2.08
$Ti_{1.2}Mn_{1.8}H_{3.0}$	6.10	7.32

[a]ref. 26, [b]estimate, [c]estimated from ref. 27, [d]estimate, [e] ref. 28, [f]ref 29, [g]estimate.

For the present initial techno-economic evaluation of the system, the shell and tube heat exchanger has been assumed as the baseline concept to exchange the needed thermal power. This is due to the fact that it is a consolidated and well known technology, which can give a reasonable indication of the heat transfer system influence on the overall system cost. The heat transfer fluid has been assumed to be flowing inside tubes with the metal hydride material packed around the tubes. Thus the overall heat transfer coefficient has been assessed based on the convective heat exchange with the heating/cooling fluid flowing inside the tubes and the conductive heat transfer determined by the metal hydride materials conductive properties and the geometry. An improved metal hydride thermal conductivity has been taken into consideration (equal to 7 W/mK), considering the use of Expanded Natural Graphite (ENG) (5 wt%) or other systems already discussed and reported in the literature.[30-32] The hydrogen weight capacity of the modified material (e.g. with inclusion of ENG) has suitably been assessed accounting for the reduced system capacity. Regarding the convective heat transfer coefficient, a value of 2000 W/m^2K has been assumed for both the HTMH and the LTMH. Regarding the HTMH system, convective heat transfer coefficients on the order of 1500 W/m^2K are reported in literature for the heat exchange between CSP system high temperature fluids (flowing inside tubes) and storage system materials.[33] Such values also depend on the operating conditions and on the heat transfer fluid. For the LTMH system, given the LTMH properties, the low temperature system heat transfer fluid will be condensing steam or liquid water (with the storage system coupled to a solar driven steam power plant). Such fluids typically allow heat transfer coefficients on the order of 1000-10000 W/m^2K (or even higher) to be achieved. Thus an overall heat transfer coefficient on the order of 400 W/m^2K (depending on the system considered) can be achieved for both high temperature and low temperature tanks.

The costs of the heat transfer and pressure vessel system have also been evaluated by adopting a factored method approach. The cost has been assessed based on the component heat transfer area and size of the vessel. In addition, suitable factors that account for the type of heat exchanger (straight fixed tubes for the present application), pressure conditions (depending on the high and low temperature metal hydrides) and material (stainless steel has been assumed as the baseline material for this application) have been adopted to evaluate the Free On Board (FOB) component cost. The database adopted to evaluate heat transfer system and pressure vessel costs are based on Reference 34. Suitable installation factors (which account for piping, insulation, painting, concrete as well as labor etc.) and cost escalation indexes have also been included in the calculations to evaluate the final component installed cost. Such installation factors have been assessed based on suitable considerations for the current application and on the available databases.[34] More details on the system economic cost assessment will also be provided as part of a future publication.[35]

3.1 Experimental Characterisation of $NaMgH_2F$

XRD of the as-milled sample (not shown) revealed only the starting reagents and trace amounts of the impurity phases MgO, Mg and NaOH (~ 4 wt.% total as determined by Rietveld refinement). XRD of the sample after annealing under hydrogen, Figure 2, shows the formation of the $NaMgH_2F$ phase consistent with that previously reported by Bouamrane et al.[15] Traces of NaH and MgO are also observed as impurity phases.

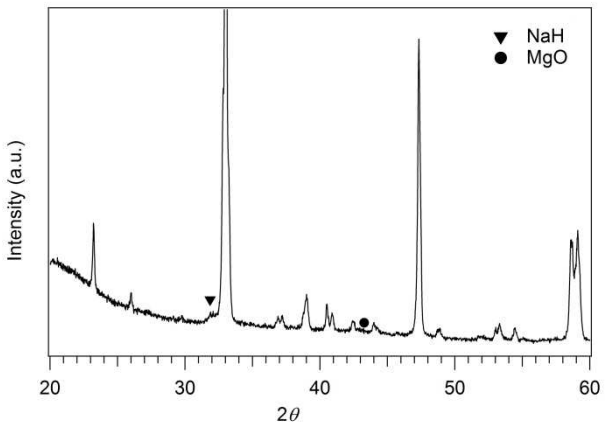

Fig 2 X-ray diffraction of $NaMgH_2F$ after annealing at 300 °C under 58 bar of H_2 overnight. All unlabelled peaks are consistent with $NaMgH_2F$.

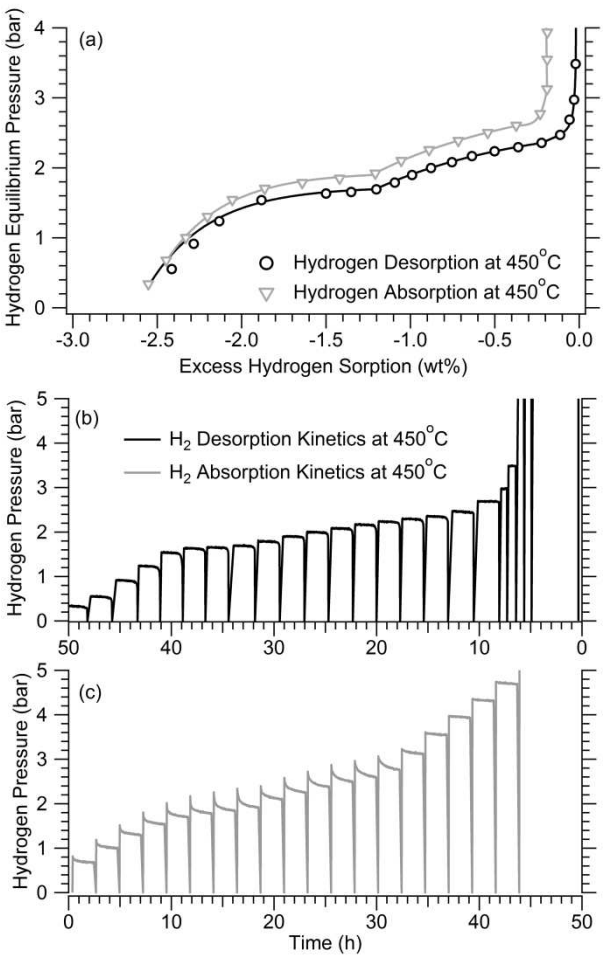

Fig 3 (a) Hydrogen desorption and absorption curves performed at 450 °C, (b) Hydrogen desorption kinetic data for the PCI curve at 450 °C and (c) Hydrogen absorption kinetic data for the PCI curve at 450 °C.

Figure 3 (a) also suggests that there is some degree of hysteresis between absorption and desorption. However, from the kinetic data for the desorption and absorption curves (Figure 3 (b) and Figure 3 (c)) it is apparent that while the desorption kinetics are quite rapid, the absorption kinetics at 450 °C are somewhat slower. Consequently, the hysteresis is an artifact of the slow absorption kinetics. The desorption kinetics of $NaMgH_2F$, even at 450 °C, appear to be fast enough for its application as a solar thermal heat storage medium where absorption kinetics are less demanding than for hydride candidates for passenger vehicles. The rehydriding kinetics appears to need improvement, with further work required at higher temperatures to determine how the kinetics change with temperature. It can also be seen in Figure 3 (a) that full rehydriding was not achieved. After complete desorption at 450 °C XRD, Figure 4(a), shows the formation of Na, Mg and $NaMgF_3$ rather than the desired phases of NaF and Mg.

XRD was also performed after incomplete rehydriding at 491 °C (Figure 4(b)) and shows only the $NaMgH_2F$ phase and a small amount of the MgO contaminant. There is no unreacted Na and Mg detectable in the XRD as would be expected from incomplete rehydriding. Upon dismantling the sample cell used for hydriding, metal deposits were found beyond the filter used to contain the sample. This result is unexpected since the lowest hydrogen pressure experienced by the sample at 491.2 °C was 0.7 bar, well above the vapor pressure of Na (5 x 10^{-3} bar)[36] and Mg (8 x 10^{-5} bar)[37] at this temperature. One potential explanation for the removal of metal from the system may be the step-wise nature of the Sieverts method used for PCI measurements. At the beginning of each step in the PCI curve there is an instantaneous hydrogen pressure differential between the sample side volume and reference side volume. The resulting transient hydrogen flow may be sufficient to act as a carrier gas for metal vapor in an analogous manner to a carrier gas in Temperature Programmed Desorption Mass Spectrometry.[38] Further work needs to be done on preventing Na and Mg loss from the sample during desorption. However, previous research on small amounts of sodium hydride has addressed this problem by using thin walled iron crucibles that are permeable to hydrogen gas but not sodium vapour.[39] The viability of this approach on a large scale would need to be verified.

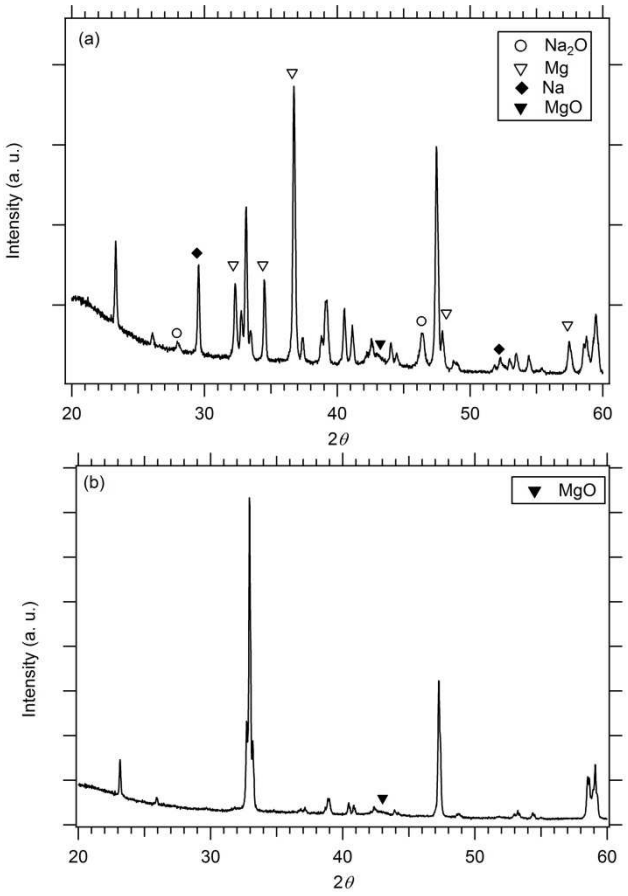

Fig 4 (a) XRD of $NaMgH_2F$ after H_2 desorption at 450 °C where unindexed peaks are $NaMgF_3$. (b) XRD of $NaMgH_2F$ after rehydriding at 491 °C where unindexed peaks are $NaMgH_2F$.

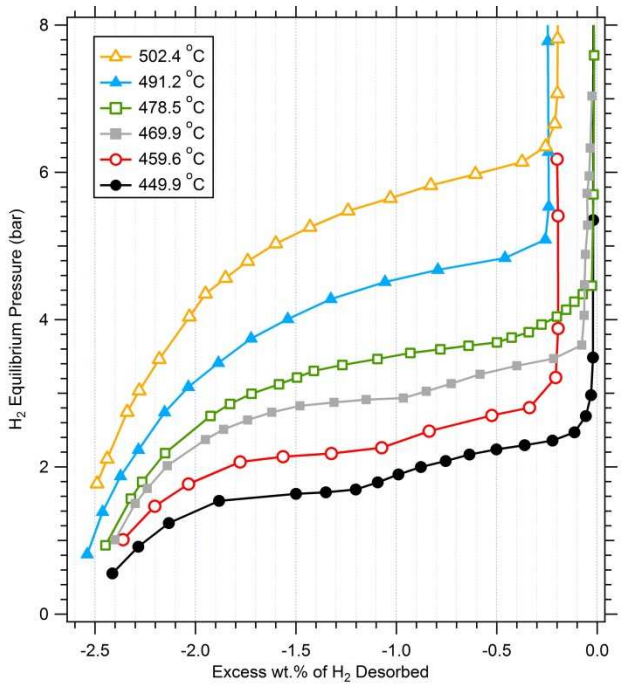

Fig 5 Hydrogen desorption Pressure-Composition-Isotherms (PCI) for $NaMgH_2F$ performed between 450 °C and 502 °C.

Hydrogen desorption PCI measurements were performed between 450 °C and 502 °C, Figure 5, in order to determine the thermodynamics of hydrogen release. Desorption measurements below 470 °C show two clear desorption processes. As the temperature increases from 450 °C to 470 °C there is a shortening of the first desorption plateau relative to the second. By 478 °C, the first plateau has almost disappeared and the desorption curves are more consistent with the hydrogen existing as a randomly distributed solid solution rather than a stoichiometric hydride phase. This lack of flat plateaux is a disadvantage from an engineering perspective where absorption and desorption of hydrogen at a constant pressure is ideal.

Because of their difference in shape, the desorption curves above and below 470 °C were treated separately for determining the thermodynamics of hydrogen release via the construction of van't Hoff plots. Each curve was numerically fitted so that the enthalpy and entropy could be determined at a consistent hydrogen content. The van't Hoff plots for hydrogen desorption values beyond -2.0 w.t% showed a poor linear fit and were not considered further. The poor fits are possibly due to small errors in the calculated leak rates that accumulate over the course of the desorption measurements that may compound at lower pressures. Figure 6 (a) shows the variation in desorption enthalpy for the PCI curves measured above and below 470 °C as a function of hydrogen content. Above 470 °C the enthalpy slowly decreases from 100.3 kJ/mol.H_2 to 92.2 kJ/mol.H_2 between H_2 desorption values of -0.5 wt.% and -2.0 wt.%.The enthalpy at the midpoint of full desorption is 96.8 kJ/mol.H_2. This is ~10 kJ/mol.H_2 higher than for $NaMgH_3$ decomposing into NaH and Mg,[7] ~20 kJ/mol.H_2 higher than for Mg_2FeH_6 and ~23 kJ/mol.H_2 higher than for MgH_2.[6] The entropy (Figure 6(b)) shows a similar trend in decreasing from 144.3 J/mol.H_2.K to 130.6 J/mol.H_2.K between desorption values of -0.5 wt.% and -2.0 wt.%.

The variation in enthalpy and entropy for desorption below 470 °C is markedly different to that at higher temperatures. The enthalpy increases from 86.8 kJ/mol.H_2 to 98.2 kJ/mol.H_2 between a desorption value of -0.4 wt.% and -1.1 wt.%. Between -1.1 wt.% and -1.2 wt.% there is a discontinuity where the enthalpy spikes to 121.4 kJ/mol.H_2 before decreasing to 104.8 kJ/mol.H_2 by -2.0 wt.% H_2 desorption. The entropy at -0.4 wt.% desorption begins at 126.9 J/mol.H_2.K and increases to 140.7 J/mol.H_2.K at -1.1 wt.% desorption. Again, there is a discontinuity between -1.1 wt% and -1.2 wt% where the entropy spikes to 172.3 J/mol.H_2.K before decreasing to 148.1 J/mol.H_2.K by -2.0 wt.% H_2 desorption.

It should be noted that, below 470 °C, the enthalpy and entropy for the beginning of each desorption plateau of $NaMgH_2F$ is similar to that observed for each plateau in the desorption of $NaMgH_3$. In the $NaAlH_4$ system doped with fluorine, Eigen et al.[40] observed partial hydrogen substitution in NaF and suggested an anion exchange mechanism between $NaF_{1-y}H_y$ and fluorine rich $Na_3AlH_{6-x}F_x$ for the release of hydrogen. In a similar manner, we propose that the first hydrogen desorption plateau below 470 °C, Equation 6, has decomposition products of fluorine enriched $NaMgH_{1+x}F_{2-x}$ and hydrogen rich $NaH_{1-x}F_x$. The second desorption plateau, is proposed to consist of anion exchange between $NaMgH_{1+x}F_{2-x}$ and $NaH_{1-x}F_x$ to form $NaMgF_3$ and H_2.

$$3NaMgH_2F \rightarrow {}^3/_2NaMgH_{1+x}F_{2-x} + {}^3/_2NaH_{1-x}F_x + {}^3/_2Mg + {}^3/_2H_2$$
$$(\text{for } x << 0.5) \rightarrow NaMgF_3 + 2Na(l) + 2Mg + {}^3/_2H_2$$

Equation 6

This was confirmed by performing a partial hydrogen desorption (-1.0 wt.%) at 450 °C. XRD of the product (not shown) revealed the presence of Mg, $NaH_{1-x}F_x$ and $NaMgH_{1+x}F_{2-x}$. The lattice parameter of the $NaH_{1-x}F_x$ was contracted slightly to 4.859 Å, compared to the as-milled NaH value of 4.880 Å, that indicates partial substitution of H for F (NaF lattice parameter is 4.632 Å). The lattice parameters of $NaMgH_{1+x}F_{2-x}$ (a = 5.477 Å, b = 7.688 Å and c = 5.393 Å) were, likewise, part-way between the original lattice parameters of $NaMgH_2F$ (a = 5.472 Å, b = 7.694 Å and c = 5.402 Å) and $NaMgF_3$ (a = 5.486 Å, b = 7.674 Å and c = 5.370 Å)

Above 478 °C the desorption reaction of $NaMgH_2F$ can be represented as a single step reaction:

$$3NaMgH_2F \rightarrow NaMgF_3 + 2Na_{(l)} + 2Mg + 3H_2$$

Equation 7

Hydrogen desorption from $NaMgH_2F$ above 478 °C occurs via the incremental concentration of F and the concurrent expulsion of Na and Mg from the perovskite phase, $NaMgH_{2-y}F_{1+y}$ (for $0 \leq y \leq 2$). The increase in stability of the perovskite $NaMgH_3$

structure as a function of fluorine substitution for hydrogen[14] and the fact that $NaMgH_3$ and $NaMgF_3$ form a complete solid solution series with H^- and F^- anions randomly distributed in the anionic sites,[15] accounts for the shape of the observed hydrogen desorption curve.

For $NaMgH_2F$ to be considered as a concentrating solar thermal storage medium, operating temperatures above 478 ^oC are likely to be used given the low hydrogen desorption equilibrium pressures below this temperature. By assuming an operating temperature above 478 ^oC, by using the enthalpy at the midpoint of the desorption plateau (96.8 kJ/mol.H_2) and by assuming a theoretical H_2 capacity of 2.95 wt.%, the theoretical thermal storage capacity of $NaMgH_2F$ was determined to be 1416 kJ/kg. This is only half the theoretical thermal storage capacity of MgH_2 (2814 kJ/mol.H_2) but, as suggested by Figure 1 and discussed below, the higher enthalpy and operating temperature of $NaMgH_2F$ results in a cost advantage when considering coupled metal hydrides for concentrating solar thermal storage.

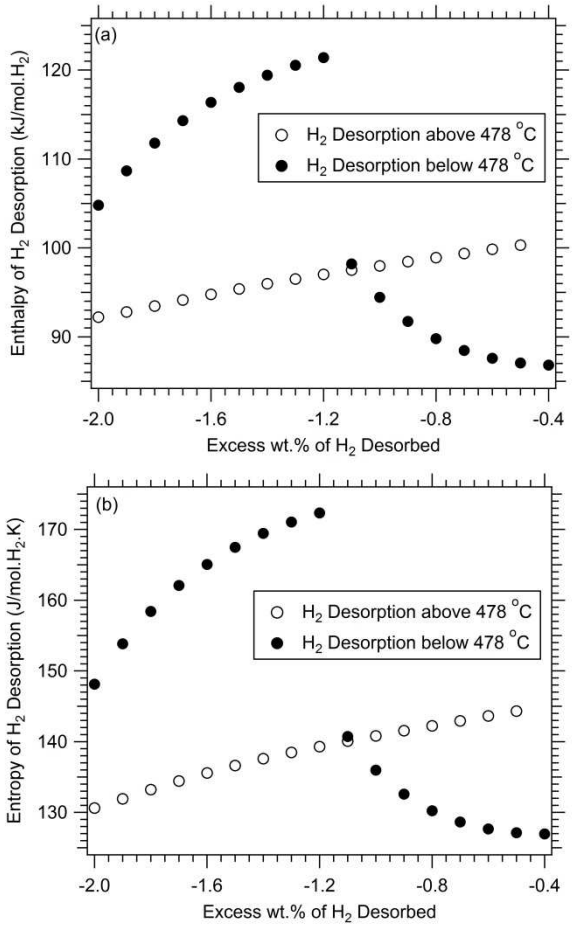

Fig 6 (a) Variation in the hydrogen desorption enthalpy and (b) variation in the hydrogen desorption entropy of $NaMgH_2F$.

3.2 Technical and Cost Assessment of Mg-based Hydrides for Concentrating Solar Power Thermal Storage

A coupled metal hydride concentrating solar thermal storage system has been considered with $NaMgH_2F$ as the HTMH and $Ti_{1.2}Mn_{1.8}H_{3.0}$ as the LTMH. Among the possible low temperature metal hydrides reported in Reference 3, this Ti-based material has been selected since it is one of the lower cost intermetallic hydrides that operates near ambient temperatures and at relatively low pressures. The performance of the $NaMgH_2F$ – $Ti_{1.2}Mn_{1.8}H_{3.0}$ system was also compared to other known Mg-based materials, such as MgH_2 and Mg_2FeH_6, as well as the recently studied $NaMgH_3$ (Table 2).

The practical hydrogen weight capacity (as indicated in Table 2) has been used in the techno-economic assessment. The difference between the practical and the theoretical capacity varies for different high temperature metal hydrides (i.e. the practical capacity of MgH_2 for solar thermal applications is only ~78 % of the theoretical value, 7.66 wt.% of H_2, while the practical capacity of Mg_2FeH_6 is ~91% of the theoretical value, 5.47 wt.% of H_2).[6] This results in a variation of the cost of the system material cost, as well as the containment volume and, hence, cost of the containment pressure vessel and heat exchanger as discussed in the following sections.

Journal Name RSCPublishing

ARTICLE

Table 2. Comparison of four Mg-based high-temperature metal hydrides (HTMH) coupled with $Ti_{1.2}Mn_{1.8}H_{3.0}$ (LTMH) for solar thermal storage for a 200 MW_{el} turbine with approximately 7 h of thermal storage when operating at full-load. ENG of 5 wt.% is included.

Material	**Theoretical/Practical H_2 wt.%**	**ΔH (*kJ/mol. H_2*)**	**Operating range (^oC)**	**Operating pressure range (*bar*)**	**Practical density (kg/m^3)**	**Thermal conductivity (*W/m.K*)**
MgH_2	7.66/6.0	74[a]	300-400	1.6-17	800[a]	7
Mg_2FeH_6	5.47/5.0	77[a]	385-470	7-37	1220[a]	7
$NaMgH_3$	4.01/3.3	86.6[b]	475-575	7-37	1000[c]	7
$NaMgH_2F$	2.95/2.5	96.8[d]	510-605	7-37	1390[d]	7
Material	**Practical thermal energy stored (MWh_{th})**	**H_2 mass (*tons*)**	**Metal mass in hydride (*tons*)**	**Mass of ENG (*tons*)**	**Metal hydride + ENG volume (m^3)**	**Heat transfer area (m^2)**
MgH_2 $Ti_{1.2}Mn_{1.8}H_{3.0}$	5132	500	7822 28771	390 1444	10048 13252	67476 32014
Mg_2FeH_6 $Ti_{1.2}Mn_{1.8}H_{3.0}$	4356	407	7739 23551	387 1178	6560 10810	54301 26115
$NaMgH_3$ $Ti_{1.2}Mn_{1.8}H_{3.0}$	3851	320	9382 18514	469 926	9594 8498	53075 20529
$NaMgH_2F$ $Ti_{1.2}Mn_{1.8}H_{3.0}$	3704	276	10746 15932	537 797	7929 7313	49574 17667

[a] ref. 6, [b] ref 7, [c] estimated, [d] This work.

The $NaMgH_2F$-system shows some promising characteristics. The hydrogen mass to be stored is almost 45% lower than that of the MgH_2 system. This is due to the higher reaction enthalpy of the $NaMgH_2F$ material (more than 30% higher than MgH_2), as well as the higher plant efficiency due to the increased operating temperature. As a consequence the LTMH mass decreases by the same percentage. However, based on the practical weight capacity of the materials, the mass of $NaMgH_2F$ material is approximately 37% higher than the corresponding MgH_2 system value, since the hydrogen weight capacity of the $NaMgH_2F$ material is about 58% lower than that of MgH_2 material. Likewise, the heat transfer area of the systems decreases, both for the high temperature and low temperature materials, with an increase in the high temperature hydride heat of reaction (i.e. decreasing of the hydrogen mass to be stored in the same storage time).

The installed costs of the four different Mg-based systems paired with $Ti_{1.2}Mn_{1.8}H_{3.0}$ are reported in Figure 7. The costs of the high temperature and low temperature material (including additional material handling and processing) and high-temperature heat exchanger and low-temperature heat exchanger (including heat exchanger and pressure vessel cost) are shown. The $NaMgH_2F$ based system shows that, despite requiring ~58 wt.% more HTMH, the overall installed cost decreases by approximately 37% compared to the corresponding MgH_2 system cost and by approximately 18% relative to the $NaMgH_3$ system. For all the selected systems, the low temperature material cost is the most significant item, representing approximately 59% of the overall $NaMgH_2F$ system cost and about 67% of the overall MgH_2 system cost. The large contribution to the overall installed cost from the LTMH considered here ($Ti_{1.2}Mn_{1.8}H_{3.0}$), despite being one of the lowest cost intermetallic hydrides, is due to a combination of both its low hydrogen capacity and the relatively high cost of titanium compared to the elements comprising the high-temperature metal hydrides. The result of this analysis is that the most effective way to reduce the overall installed cost of a coupled metal hydride concentrating solar thermal storage system is to reduce the quantity of hydrogen to be stored. This results in a decrease of: 1) the LTMH material cost, and 2) the LTMH heat exchanger cost, due to the decrease of the thermal power to be exchanged. The LTMH heat exchanger cost decrease from the MgH_2 to the $NaMgH_2F$ system is on the order of 30%. With the assumptions made to evaluate the costs, regarding the HTMH costs: 1) the HTMH material cost when changing from MgH_2 to $NaMgH_2F$, decreases by almost 23%, mainly due to the reduced raw material cost and the amount of hydrogen required to be stored, despite the reduced weight capacity of the $NaMgH_2F$ system compared to MgH_2; 2) the HTMH heat exchanger and pressure vessel cost when changing from MgH_2 to $NaMgH_2F$, decreases by about 18.5%, mainly due to the reduction of the thermal power to be exchanged and the decrease of the total volume (because of the higher material density).

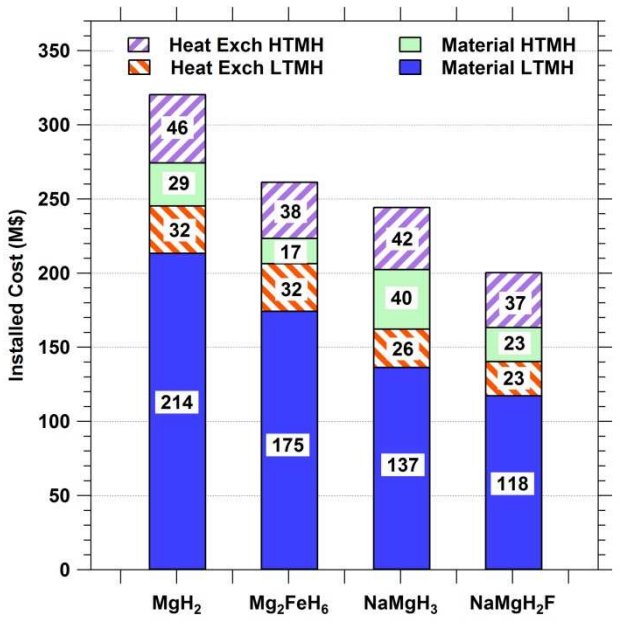

Fig 7 Installed costs of four solar thermal storage systems comprised of Mg-based hydrides coupled with $Ti_{1.2}Mn_{1.8}H_{3.0}$ for 7 hours of thermal storage for a 200 MW_{el} turbine. The costs of materials for the high-temperature metal hydrides and low-temperature metal hydrides, which is based on the processed material cost (including the raw material cost plus additional costs due to material handling, processing and placement in the vessel) are denoted as Material HTMH and Material LTMH, respectively. The installed cost of the heat exchanger and pressure vessel systems for the high-temperature metal hydrides and low-temperature metal hydrides are denoted as Heat Exch HTMH and Heat Exch LTMH, respectively.

Based on this cost analysis, $NaMgH_2F$ has advantages over the well-studied MgH_2 as a solar thermal storage material that include: a higher enthalpy of hydrogen absorption/desorption; a higher operating temperature; a reduction in the quantity and cost of LTMH required, that also reduces the volume and cost of the LTMH containment vessel and; a higher practical density that reduces the volume and cost of the HTMH containment vessel. The disadvantages of $NaMgH_2F$ compared to MgH_2 include: a sloping plateau; insufficient hydrogen absorption kinetics at 450 ^oC and; some loss of metallic sodium and magnesium from the system upon hydrogen cycling. Whilst the sloping plateau is an intrinsic feature of $NaMgH_2F$, the potential cost savings of $NaMgH_2F$ over other Mg-based hydrides means that further work on improving the kinetics of hydrogen absorption and minimizing sodium and magnesium loss and assessment of the long term cyclic stability of $NaMgH_2F$ is required.

The analysis reported here represents a preliminary techno-economic assessment of the proposed storage system ($NaMgH_2F$) with the aim of comparing its performance with that of the other Mg-based metal hydride storage systems. All the coupled systems show a preliminary specific cost on the order of 50-60 $/kWhth. This cost is on the same order of the values available in the literature for molten salt technology [41,42] which range from 30 to 80 $/kWhth but a more thorough assessment taking into account the levelised cost of energy (LCOE) is required. However, the new storage system presented here is based on typical current values of the CSP plant properties (e.g. power plant efficiencies, storage time, plant capacity factor, etc.) and only consolidated technologies are examined (e.g. typology of heat exchangers, materials, etc.). Possible future techno-economic improvements of the CSP plant, which result in a remarkable reduction of the system installed cost, will be considered as part of another publication.[35] Additional factors that could influence the ultimate cost of a concentrating solar thermal storage system based on coupled metal hydrides include: (1) an assessment of the kinetics of paired metal hydride systems, as differences in hydrogen absorption/desorption kinetics between the paired metal hydrides may place additional constraints/costs on the system; (2) variations in the practical achievable densities of metal hydride powders compacted with ENG needs to be considered and explored; (3) the slope of the hydrogen absorption/desorption curve/plateau (such as for $NaMgH_2F$) that can result in parasitic energy losses; (4) the heat capacities of the metals/metal hydrides, ENG and shell/tube/heat exchangers that have not been included in this assessment and would serve to act as thermal ballast and decrease the quantity and cost of metal hydrides required and; (5) the hydrogen equilibrium pressure of an intermetallic LTMH that may need to be altered by the addition of suitable transition metals (such as, Ti, Zr, V, Cr or Fe as some possible examples) that may increase its cost.

4. Conclusions

A simplified techno-economic model has been applied as a screening tool for metal hydrides as concentrating solar thermal heat storage materials. The installed cost of four magnesium-based high-temperature metal hydride (HTMH) systems (MgH_2, Mg_2FeH_6, $NaMgH_3$ and $NaMgH_2F$) paired with $Ti_{1.2}Mn_{1.8}H_{3.0}$ as a low-temperature metal hydride hydrogen store, have been assessed. For the first time the hydrogen storage properties of $NaMgH_2F$ have been examined and it has a practical hydrogen capacity of 2.5 wt% (theoretical: 2.95 wt% H_2), a sloping single-step hydrogen desorption curve above 478^oC, a plateau mid-point enthalpy of 96.8 kJ/mol.H_2 and a thermal storage capacity of 1416 kJ/kg. The techno-economic model revealed that, despite the lowest thermal storage capacity of the magnesium-based hydrides considered here, the high enthalpy and operating temperatures of $NaMgH_2F$ means that substantially less hydrogen is required for generating electric power compared to other Mg-based hydrides for solar thermal storage. The high cost of ambient temperature (in the LTMH) H_2 storage results in a significant cost advantage for $NaMgH_2F$ over other magnesium-based hydrides for solar thermal storage. Further research on $NaMgH_2F$ is needed to address the sluggish hydrogen absorption kinetics as well as the loss of sodium and magnesium metal from the system upon H_2 cycling

Acknowledgements

C.E.B, D.A.S and M.P. acknowledge the financial support of the Australian Research Council (ARC) for ARC Linkage grant LP120101848 and C.E.B. also acknowledges ARC LIEF grants LE0989180 and LE0775551, which enabled the XRD and gas sorption studies to be done. C.C, B.H, T.M and R.Z acknowledge the U.S. Department of Energy, Office of Energy Efficiency and Renewable Energy, and the SunShot Initiative.

Notes and references

[a] Hydrogen Storage Research Group, Fuels and Energy Technology Institute, Department of Imaging and Applied Physics, Curtin University, GPO Box U1987, Perth, WA 6845, Australia

[b] Savannah River National Laboratory, 999-2W, Aiken, SC, 29808, USA

References

1 D. Abbott, *Proc IEEE,* 2010, **98**, 42.
2 R. Passey, M. Watt, *EcoGeneration Mag*, 2010, 82.
3 D.N. Harries, M. Paskevicius, D.A. Sheppard, T.E.C. Price, C.E. Buckley, *Proc. IEEE.*, 2012, **100**, 539.
4 HSC software version 6.12, Outotec Research Oy, 1974 – 2007.
5 S.D. Sharma, K. Sagara, *Int. J. Green Energy*, 2005,**2**, 1.
6 A. Reiser, B. Bogdanović, K. Schlichte, *Int. J. Hydrogen Energy,* 2000, **25**, 425.
7 D.A. Sheppard, M. Paskevicius, C.E. Buckley, *Chem. Mater.,* 2011, **23**, 4298.
8 E.S. Freeman, *J. Phys. Chem*., 1956, **60**, 1487.
9 M. Fellet, C.E. Buckley (*Ed*), M. Paskevicius (*Ed*), D.A. Sheppard (*Ed*), *MRS Bulletin Energy Quaterly*, 2013, **38**, 1012.
10 R.F. Boehm, *Appl. Energy*., 1986, **23**, 281.
11 J.J. Reilly, R.H. Wiswall, *Inorg. Chem*., 1978, **7**, 2254.
12 J. Sangster, A.D. Pelton, H-Li (Hydrogen-Lithium) *in* Phase Diagrams of Binary Hydrogen Alloys 2000;74 – 82, F.D. Manchester (*Ed*), ASM International, Ohio, 2000.
13 E. Rönnebro, D. Noréus, K. Kadir, A. Reiser, B. Bogdanović, *J. Alloys. Compnds*., 2000, **299**, 101.
14 A. Bouamrane, C. de Brauer, J.-P. Soulié, J.M. Létoffeé, J.P. Bastide, *Thermochem. Acta.*, 1999, **326**, 37.
15 A. Bouamrane, J.P. Laval, J.-P. Soulié, J.P. Bastide, *Mater. Res. Bulletin*, 2000, **35,** 545.
16 D. Pottmaier, E.R. Pinatel, J.G. Vitillo, S. Garroni, M. Orlova, M.D. Baró, G.B.M Vaughan, M. Fichtner, W. Lohstroh, M. Baricco, *Chem. Mater*., 2011, **23**, 2317.
17 K. Komiya, N. Morisaku, R. Rong, Y. Takahashi, Y. Shinzato, H. Yukawa, M. Morinaga, *J. Alloys Compnds*., 2008, **453**, 157.
18 T. Gamo, Y. Moriwaki, N. Yanagihara, T. Yamashita, T. Iwaki, *Int. J. Hydrogen Energy*, 1985, **10**, 39.
19 M. Paskevicius, D.A. Sheppard, C.E. Buckley, *J. Am. Chem. Soc.*, 2010, **132**, 5077.
20 C. San Marchi (*Ed*), B. Somerday (*Ed*), S. Robinson (*Ed*), Sandia National Laboratories Technical Report WSRC-STI-2007-00579 prepared under Contract No. DE-AC09-96SR18500 with the U.S. Department of Energy. 2005;1 – 31.
21 US Department of Energy "SunShot Vision Study, Chapter 5: Concentrating Solar Power: Technologies, Cost, and Performance" February 2012.
22 T. Gamo, T. Moriwaki, N. Yanagihara, T. Iwaki, *J. Less-Common Metals*, 1983, **89**, 495.
23 B. Bogdanović, H. Hofmann, A. Neuy, A. Reiser, K. Schlichte, B. Spliethoff, S. Wessel, *J. Alloys Compnds*., 1999, **292**, 57.
24 K.M. Guthrie, *Chem. Eng. Progr*., 1969, 114.
25 T. Motyka, Savannah River National Laboratory Regenerative Fuel Cell Project. SRNL-STI-2008-00388, Nov. 11, 2008.
26 Cost for 99.8% Mg (http://www.metalprices.com/metal/magnesium/magnesium-99-9-usa) = US$3.0/kg as of 9/11/11. Accessed 11th January 2013
27 DiPietro JP, Skolnik EG. US Department of Energy, Office of Power Technologies, 1999. Available online: http://www.eere.energy.gov/hydrogenandfuelcells/pdfs/28890pp2.pdf . Accessed: 16th of March 2011.
28 Available online at www.metalprices.com/historical/database/manganese/manganese-electrolytic-metal-99-7-rotterdam. Manganese Price is for March 2012. Accessed 19th of April 2013.
29 Available online at www.metalprices.com/historical/database/titanium/titanium-sponge-rotterdam-fob. Price is for November 2011 to March 2012. Accessed 19th of April 2013.
30 A. Chaise, P. de Rango, P. Marty, D. Fruchart, S. Miraglia, R. Olivès, S. Garrier, *Int. J. Hydrogen Energy*, 2009, **34**, 8589.
31 C. Corgnale, B. Hardy, S. Garrison, D. Tamburello, D. Anton, *Int. J. Hydrogen Energy*, 2012, **37**, 2812.
32 J.M. Pasini, C. Corgnale, B. Van Hassel, T. Motyka, S. Kumar, K. Simmons, *Int. J. Hydrogen Energy*, 2013, **38**, 9755.
33 C. Corgnale, W. Summers, *Int. J. Hydrogen Energy*, 2011, **36,** 11604.
34 E. Douglas, "Industrial Chemical Process Design" McGraw-Hill Professional Engineering, 2003.
35 C. Corgnale, B. Hardy, T. Motyka, R. Zidan, J. Teprovich, B. Peters, *Submitted* to *Renewable and Sustainable Energy Reviews*.
36 M.W. Makansi, C.H. Muendel, W.A. Selke, *J. Phys. Chem.*, 1955, **59**, 40.
37 J. F. Smith, R.L. Smythe, *Acta Metallurgica*, 1959, **7,** 261.
38 D.A. Sheppard, M. Paskevicius, C.E. Buckley, *J. Phys. Chem. C.*, 2011, **115,** 8407.
39 M. D. Banus, J.J. McSharry, E.A. Sullivan, *J. Am. Chem. Soc.*, 1955, **77**, 2007.
40 N. Eigen, U. Bösenberg, J. Bellosta von Colbe, T.R. Jensen, T. Cereniusc, M. Dornheim, T. Klassen, R. Bormann, *J. Alloys Compnds*., 2009, **477**, 76.
41 C. Turchi, M. Mehos, C. K. Ho, G. J. Kolb, National Renewable Energy Laboratory Report NREL/CP-5500-49303, October 2010.
42 G. Kolb, C. K. Ho, T. Mancini, J. Gary, Sandia Report SAND2011-2419, April 2011.

Table of Contents Entry

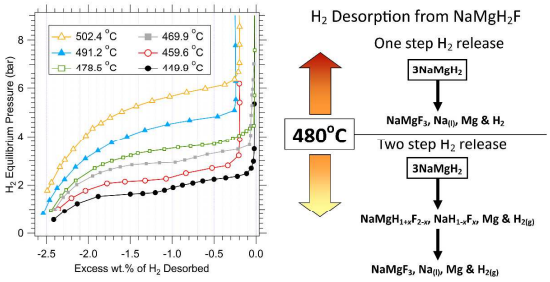

An economic assessment is performed on $NaMgH_2F$ and magnesium-based metal hydrides as heat storage materials for concentrating solar thermal power.